



1 Characterization of secondary organic aerosol from heated- 2 cooking oil emissions: evolution in composition and volatility

3 Manpreet Takhar¹, Yunchun Li², Arthur W. H. Chan¹

4 ¹Department of Chemical Engineering and Applied Chemistry, University of Toronto, Toronto, M5S 3E5, Canada

5 ²College of Science, Sichuan Agricultural University, Ya'an, 625014, China

6 *Correspondence to:* Arthur W. H. Chan (arthurwh.chan@utoronto.ca)

7 **Abstract.** Cooking emissions account for a major fraction of urban organic aerosol. It is therefore important to
8 understand the atmospheric evolution in the physical and chemical properties of organic compounds emitted from
9 cooking activities. In this work, we investigate the formation of secondary organic aerosol (SOA) from oxidation of
10 gas-phase organic compounds from heated cooking oil. The chemical composition of cooking SOA is analyzed using
11 thermal desorption-gas chromatography-mass spectrometry (TD-GC/MS). While the particle-phase composition of
12 SOA is a highly complex mixture, we adopt a new method to achieve molecular speciation of the SOA. All the GC
13 elutable material is classified by the constituent functional groups, allowing us to provide a molecular description of
14 its chemical evolution upon oxidative aging. Our results demonstrate an increase in average oxidation state (from -0.6
15 to -0.24), and decrease in average carbon number (from 5.2 to 4.9) with increasing photochemical aging of cooking
16 oil, suggesting that fragmentation reactions are key processes in the oxidative aging of cooking emissions within 2
17 days equivalent of ambient oxidant exposure. Moreover, we estimate that aldehyde precursors from cooking emissions
18 account for a majority of the SOA formation and oxidation products. Overall, our results provide insights into the
19 atmospheric evolution of cooking SOA, a majority of which is derived from gas-phase oxidation of aldehydes.

20

21 1 Introduction

22 Organic aerosol (OA) has important impacts on air quality, climate and human health (Hallquist et al., 2009). OA is
23 often composed of thousands of organic compounds formed from a variety of sources. In urban areas, particulate
24 emissions from food cooking account for a significant fraction of OA (Allan et al., 2010; Crippa et al., 2013; Florou
25 et al., 2017; Kostenidou et al., 2015; Lee et al., 2015; Mohr et al., 2012; Sun et al., 2011). Furthermore, volatile organic
26 compounds (VOCs) are also emitted, and they can undergo oxidation and form secondary organic aerosol (SOA).
27 Recent studies have reported the formation of SOA from meat charbroiling (Kaltsonoudis et al., 2017a) and heated
28 cooking oils (Liu et al., 2017b, 2017c, 2018). Therefore, food cooking activities have substantial impacts on air quality
29 in and downwind of urban areas.

30 The emission of VOCs from cooking is highly variable and depends on a number of factors such as cooking style,
31 food, ingredients, and temperature (Fullana et al., 2004a, 2004b; Klein et al., 2016a, 2016b; Liu et al., 2017c; Schauer
32 et al., 1999, 2002). Of the different classes of VOCs characterized in these studies, aldehydes have been shown to be



33 the major group of VOCs emitted from cooking oils. These VOCs are chemically produced upon heating via peroxy
34 radical reactions of the fatty acids (Choe and Min, 2007; Gardner, 1989). Klein et al. (2016a) investigated the
35 composition of nonmethane organic gas (NMOG) emissions from boiling, charbroiling, shallow and deep frying of
36 various vegetables, meats, and cooking oils heated under different temperature conditions. The authors reported that
37 emissions from shallow frying, deep frying and charbroiling are dominated by aldehydes, and the relative amounts
38 depend on the type of oil used during cooking (Klein et al., 2016a). C7 aldehydes are the major species in emissions
39 from canola oil, whereas C9 aldehydes are dominant from olive oil (Klein et al., 2016a). These differences in emission
40 patterns of oils vary with composition of triglycerides present in the oil (Choe and Min, 2006). Katragadda et al.
41 (2010) demonstrated up to an order of magnitude increase in emissions upon reaching the smoke point of cooking
42 oils. In addition to emissions from cooking oil, the addition of condiments (herbs and peppers) to cooking leads to
43 significant emissions of mono-, sesqui- and diterpenes in the gas phase (Klein et al., 2016b). Liu et al. (2017a) showed
44 an order of magnitude increase in the emissions of VOCs when stir-frying with spices. Therefore, factors like cooking
45 style, food, cooking temperature, and ingredients play a significant role in the chemical profile of cooking emissions
46 (Fullana et al., 2004a, 2004b; Klein et al., 2016a, 2016b; Liu et al., 2017a, 2017c).

47 The VOCs emitted from cooking have been shown to produce significant amount of SOA rapidly in recent flow tube
48 (Liu et al., 2017b) and smog chamber studies (Kaltsonoudis et al., 2017a; Liu et al., 2017c, 2018). Kaltsonoudis et al.
49 (2017a) and Liu et al. (2017b, 2018) showed an increase in O/C ratio upon a few hours of atmospheric aging suggesting
50 lightly oxidized cooking SOA. Furthermore, Liu et al. (2017b) showed significant production of SOA with increasing
51 OH exposure for different cooking oils. Thus far studies have only focused on formation potential of SOA from
52 cooking emissions. Despite high emission rates of VOCs from cooking, the understanding of SOA composition from
53 these emissions remains limited.

54 Source apportionment using aerosol mass spectrometry (AMS) data in urban areas has often revealed a Cooking
55 Organic Aerosol (COA) factor, but it is unclear how this factor is related to cooking emissions. Many studies reported
56 that the mass spectra associated with this factor resemble that of hydrocarbon-like organic aerosol (HOA) factor from
57 other non-cooking sources (Dall'Osto et al., 2015; Hayes et al., 2013; Huang et al., 2010; Mohr et al., 2009, 2012). In
58 addition, it is often unclear whether ambient COA represents primary or secondary organic aerosol from cooking
59 emissions (Dall'Osto et al., 2015; Florou et al., 2017; Kaltsonoudis et al., 2017b; Kostenidou et al., 2015). Laboratory
60 studies (Liu et al., 2017b, 2018) showed that the mass spectra for primary cooking organic aerosol exhibited strong
61 correlation with ambient COA factor (Lee et al., 2015), but the cooking SOA mass spectra showed some similarities
62 to ambient semi-volatile oxygenated OA (SV-OOA) factor. These measurements highlight the challenges in assigning
63 COA factor without understanding the changes in chemical composition occurring during oxidation of cooking
64 emissions.

65 In general, there is a need to better understand the molecular composition contributing to aged COA. In this study, we
66 investigate detailed chemical composition of cooking SOA at the molecular level. The objectives of this study are to:
67 (i) understand the detailed chemical speciation of cooking SOA using TD-GC/MS, (ii) describe chemical evolution in
68 SOA upon atmospheric aging, and (iii) attribute formation of SOA to different VOCs emitted from food cooking



69 emissions. In this work we use heated cooking oil as a model for food cooking emissions. We show that the majority
70 of the SOA is derived from oxidation of aldehydes, and the oxidation mechanisms are dominated by fragmentation
71 reactions. Overall, our results provide useful insights into the evolution of cooking SOA, which may be incorporated
72 into chemical transport models for better predicting OA formation from cooking emissions in the atmosphere.

73

74 2 Experimental methods

75 2.1 Flow tube experiments

76 The experimental setup is shown in Fig. 1, and experimental conditions are listed in Table S1. For each experiment,
77 30-40 mL of canola oil was heated at 250 °C on an electric heating plate in a Pyrex bottle resulting in an average
78 cooking oil temperature of 180 °C, as measured by a thermocouple in direct contact with the heated oil. Purified air
79 flowed over the headspace of the heated oil at a rate of 0.2 L min⁻¹ and then diluted by a factor of 50. 0.2 L min⁻¹ of
80 the total diluted flow was passed through a Teflon filter to remove particles, and the oil vapors were introduced into a
81 custom-built 10 L quartz flow tube reactor. A separate flow of oxygen (99.6%) was irradiated in a UV ozone generator
82 (UVP 97006601) to produce ozone and was also introduced into the flow tube reactor. In parallel, purified air was
83 flowed through a water bubbler into the reactor to provide water vapor. The combined flow rate through the flow tube
84 was set at 3 L min⁻¹, resulting in an average residence time of approximately 200 s.

85 In the flow tube, hydroxyl radicals were produced through the photolysis of ozone irradiated by a UV lamp ($\lambda = 254$
86 nm) in the presence of water vapor. The integrated OH exposure was measured indirectly from the loss of cyclopentane
87 which was monitored by a gas chromatography-flame ionization detector (GC-FID, model 8610C, SRI Instruments
88 Inc.) equipped with a Tenax TA trap sampling downstream of the flow tube at a rate of 0.15 L min⁻¹. In this study, the
89 experiments were conducted at different OH exposures ranging from 5.77×10^{10} to 2.2×10^{11} molecules cm⁻³ s. OH
90 exposure in this range is equivalent to ~11 to 41 h of atmospheric oxidation, respectively, assuming a 24-h average
91 atmospheric OH concentration of 1.5×10^6 molecules cm⁻³ (Mao et al., 2009).

92 Downstream of the flow tube, pre-baked quartz fiber filter and Tenax tube samples were collected for offline chemical
93 analysis. The changes in the particle size distribution and volume concentration were monitored using a scanning
94 mobility particle sizer (SMPS) with a differential mobility analyzer (TSI 3081), and a condensation particle counter
95 (TSI 3781). A constant density of 1.4 g cm⁻³ was assumed to convert particle volume concentration into mass
96 concentration (Chan et al., 2010). Relative humidity and temperature were monitored by an Omega HX94C RH/T
97 transmitter and were maintained at 65-70%, and 19-20 °C, respectively for all experiments. A fast stepping/scanning
98 thermodenuder (TD, Aerodyne Inc. Billerica, USA) was also placed downstream of the flow tube to measure SOA
99 evaporation rates. Details about TD operating conditions and analysis can be found in Takhar et al. (2019). The TD
100 was only operated during one experiment in which the OH exposure was 9.23×10^{10} molecules cm⁻³ s. The SOA was
101 systematically heated in a TD from 25 °C to 175 °C, and changes in particle volume concentrations and corresponding
102 mass fraction remaining (MFR) were measured using a SMPS. The SOA size distribution during TD operation and



103 volatility distribution are shown in Fig. S1 and S2, respectively. A kinetic mass transfer model developed by Riipinen
104 et al. (2010) was used to interpret the TD data. The inputs to the model are volatility distribution of OA, enthalpy of
105 vaporization, mass accommodation coefficients. Compound groups are translated into volatility distributions by
106 binning components according to their saturation concentrations (Donahue et al., 2006). Parameterization for enthalpy
107 of vaporization was similar to that of Takhar et al. (2019). We assume a surface tension of 0.05 N m^{-1} , gas-phase
108 diffusion coefficients of $5 \times 10^{-6} \text{ m}^2 \text{ s}^{-1}$ for all simulations similar to that reported in Riipinen et al. (2010).

109

110 2.2 Chemical characterization of SOA

111 Tenax tube and quartz filter samples were analyzed separately by thermal desorption gas chromatography mass
112 spectrometry (TD-GC/MS) for detailed chemical speciation of gas- and particle-phase organic compounds. The
113 analyses were performed using a thermal desorption system (TDS 3, Gerstel) combined with a gas chromatography
114 (7890B, Agilent)-mass spectrometer (5977A, Agilent). For gas-phase analysis, concentrations of aldehydes (C7 to
115 C10 *n*-alkanal, alkenals and alkadienals) collected on Tenax tube samples before photooxidation (downstream of the
116 flow tube, with lights off) were quantified. For particle-phase analysis, thermal desorption of quartz filters was
117 performed with *in situ* derivatization using *N*-trimethylsilyl-*N*-methyl trifluoroacetamide (MSTFA). A known amount
118 of deuterated 3-hydroxy-1,5-pentanedioic-2,2,3,4,4-d₅ acid, and *n*-pentadecane-d₃₂ (CDN isotopes) was injected,
119 respectively, onto quartz filter punches, and Tenax tubes as internal standards before the samples were desorbed in
120 the TDS. All GC/MS analysis was performed using a non-polar DB5 column (Rxi-5Sil MS, Restek). Details of the
121 operating parameters (GC column, GC and TDS temperature ramps, MS parameters) can be found in Sect. 1 of SI.

122 With *in situ* derivatization, polar organic compounds react rapidly with MSTFA at elevated temperatures during
123 thermal desorption, and functional groups with acidic hydrogen atoms (such as –OH) are replaced by a less polar
124 trimethylsilyl (TMS, [–OSi(CH₃)₃]) group. This reduction in polarity allows the derivatized analyte to elute from a
125 non-polar column and analyzed by subsequent electron impact (EI) at 70 eV. Derivatized compounds produce a
126 signature fragment ion at mass-to-charge (*m/z*) 73 (–Si(CH₃)₃⁺) arising from the scission of O–Si bond in R–O–
127 [Si(CH₃)₃]. In other words, all derivatized compounds produce ions with *m/z* 73 during analysis. Therefore, the total
128 signal at *m/z* 73 can be taken as the total concentration of organic compounds with at least one hydroxyl group
129 (including both –OH and –C(O)OH) present in cooking SOA, much like how *m/z* 57 represents total concentration of
130 aliphatic compounds in hydrocarbon mixtures (Zhao et al., 2014, 2015). It should be noted that organic peroxides (R–
131 OOH) were also found to be derivatized, but the major reaction product formed is R–O–[Si(CH₃)₃] (which is also
132 formed from R–OH derivatization) as shown in Fig. S3. Here we assume alcohols and acids are the major components,
133 but will explore the potential role of ROOH on the overall chemical composition in Sect. 3.1.

134 As shown in Fig. 2, many compounds in cooking SOA contain at least one –OH group and the chromatogram of *m/z*
135 73 is typical of that for a highly complex mixture or unresolved complex mixture (UCM). Using traditional analytical
136 techniques like GC/MS it is difficult to deconvolute the UCM. However, knowledge about mass spectral



137 fragmentation of TMS derivatives can be used to understand the compounds contributing to the UCM. Table S2 shows
138 a list of compounds containing multiple functional groups e.g. -COOH, -OH resulting in different combinations of
139 compound classes like dicarboxylic acids, hydroxy acids, hydroxy dicarboxylic acids, and dihydroxy dicarboxylic
140 acids with different carbon numbers. As mentioned earlier, we acknowledge the potential contribution from ROOH,
141 but will first assume the functional groups shown in Table S2 here, and consider ROOH in more detail in a later
142 section. The compound groups shown in Table S2 are expected to be formed from oxidation of aldehydes and be
143 derivatized by MSTFA. The TMS derivatives of these compounds share common ion fragments in their EI mass
144 spectra: m/z 73 $[\text{Si}(\text{CH}_3)_3]^+$, 75, 147 $[(\text{CH}_3)_2\text{Si}=\text{O}(\text{CH}_3)_3]^+$, M-15 $[\text{M}-\text{CH}_3]^+$ (Jaoui et al., 2004, 2005; Yu et al., 1998).
145 Most importantly, all TMS derivatives exhibit quantifiable peaks at m/z 73 (ubiquitous ion for all derivatives) and M-
146 15 (ion specific to each compound group, hereby referred to as the pseudo-parent ion). We also obtained the
147 characteristic ratio of these two ions for each compound group ($f_{M-15/73}$) from NIST mass spectral libraries and from
148 analyzing authentic standards. To verify the validity of this method, we calculate the total m/z 73 ion signal that is
149 attributable to these compound groups by taking the chromatograms of the pseudo-parent ion for each compound
150 group, dividing by its characteristic ratio $f_{M-15/73}$ and then summing across all compound groups as shown in Eq.
151 (1).

$$152 \quad S_{73,t}^{sum} = \sum_i \frac{S_{M-15,i,t}}{f_{M-15/73,i}} \quad (1)$$

153 where $S_{73,t}^{sum}$ is the m/z 73 ion signal at retention time t that is attributable to all compound groups listed in Table S2,
154 $S_{M-15,i,t}$ is the signal of the pseudo-parent ion for compound group i at retention time t , $f_{M-15/73,i}$ is the characteristic
155 ratio of pseudo-parent ion to m/z 73. This approach is similar to that described in Isaacman-VanWertz et al. (2020).
156 As shown in Fig. 2, $S_{73,t}^{sum}$ shows excellent agreement with the measured m/z 73 ion signal, suggesting that the m/z 73
157 signal, which is representative of all TMS derivatives, is almost entirely comprised of contributions from the
158 compound groups listed in Table S2. This agreement between our bottom-up approach and measured signal provides
159 confidence that our method is able to provide information about the chemical composition of highly complex mixture.

160 With the signals from all the pseudo parent ions for all compound groups, the total mass of each compound group was
161 then calculated using Eq. (2).

$$162 \quad M_i = \frac{TA_i}{RF_i} \times \frac{1}{f_{M-15/73,i}} \quad (2)$$

163 where, M_i is the mass of compound group i , TA_i is the total integrated signal of pseudo-parent ion for compound
164 group i (normalized by the signal of deuterated internal standard), RF is the response factor (calculated from
165 calibration curves of fatty acids and dicarboxylic acids authentic standards) of compound group i , and $f_{M-15/73,i}$ is
166 the characteristic ratio of pseudo-parent ion to m/z 73 for compound group i . A more detailed, step-by-step description
167 of the procedure can be found in the SI in Sect. 2, and illustrated in Fig. S4 with corresponding uncertainties in the
168 fitting procedure shown in Fig. S5.



169

170 3 Results and discussion

171 3.1 Chemical evolution of SOA

172 As described in Sect. 2.2, components in cooking SOA were classified by functional groups and carbon number. To
173 describe the overall changes in SOA composition with increasing OH exposure, we use the average carbon oxidation
174 state ($\overline{\text{OSc}}$) as a metric for the evolving composition of a complex mixture undergoing oxidation (Kroll et al., 2011).
175 Both $\overline{\text{OSc}}$ and number of carbon atoms (nc) for each compound group are calculated from the GC-derived chemical
176 composition. The total mole fraction of C, H and O was calculated for each sample which was then used to calculate
177 the bulk $\overline{\text{OSc}}$ using the Eq. $2 \times O:C - H:C$ (Kroll et al., 2011). The evolution in this framework for canola oil SOA
178 is shown in Fig. 3. The bulk $\overline{\text{OSc}}$ was observed to increase from -0.6 to -0.24 when OH exposure increased from 5.77
179 to 22.0×10^{10} molecules cm^{-3} s for canola oil SOA. For comparison, Liu et al. (2017b) showed an initial decrease in
180 $\overline{\text{OSc}}$ and O:C, but gradually stabilized at OH exposure greater than 9×10^{10} molecules cm^{-3} s. For the $\overline{\text{OSc}}$ range reported
181 here, the $\overline{\text{OSc}}$ of cooking SOA falls in the range of SV-OOA as determined from factor analysis of AMS data
182 (Canagaratna et al., 2015). This degree of oxygenation is greater than that of the COA factor measured by AMS, which
183 is reported to be around -1.37 (Canagaratna et al., 2015). This difference suggests that the COA factor resolved using
184 PMF analysis is likely of primary origin and does not represent SOA formed from atmospheric oxidation of cooking
185 emissions. Furthermore, previous GC/MS analysis showed for POA from cooking oils, an $\overline{\text{OSc}}$ of -1.66 (canola oil)
186 and -1.7 (beef tallow, olive oil) was calculated (Takhar et al., 2019). These observations again suggest that COA factor
187 measured by AMS is derived of primary cooking emissions.

188 In addition to carbon oxidation state, knowledge about molecular composition provides further insights into the
189 oxidation mechanisms. Canola oil SOA at an OH exposure of 5.77×10^{10} molecules cm^{-3} s is comprised of long chain
190 hydroxy acids, whereas at higher OH exposure more short-chain dicarboxylic acids and hydroxy dicarboxylic acids
191 are produced. As a result, oxidation simultaneously leads to higher $\overline{\text{OSc}}$ and lower carbon number on average. Based
192 on the compounds observable by our technique, this trend suggests that fragmentation reactions are key processes in
193 the oxidative evolution of cooking emissions. These findings suggest an early onset of fragmentation reactions upon
194 atmospheric aging of cooking emissions contrary to other SOA systems, such as alkanes and isoprene (Lambe et al.,
195 2012, 2015), in which fragmentation reactions dominate at later OH exposures ($> 5 \times 10^{11}$ molecules cm^{-3} s). Therefore,
196 predicting OA concentrations from cooking emissions would require earlier fragmentation of SOA in climate and air
197 quality models.

198 The compounds observed here can also be compared to previously measured bulk composition using elemental ratios,
199 such as those presented in a Van Krevelen (VK) diagram (Heald et al., 2010). As shown in Fig. 4, the O:C ratio in our
200 study ranged between 0.64 and 0.79 when OH exposure increased from 5.77×10^{10} to 22.0×10^{10} molecules cm^{-3} s.
201 These ratios are within a factor of 2 than previously reported AMS measurements of cooking oil SOA (Kaltsonoudis
202 et al., 2017a; Liu et al., 2017b). Furthermore, the H:C versus O:C trend is linear with a slope of -0.19, which lies



203 between the slope of 0 measured for low-NO_x oxidation reported by Liu et al. (2017b) and -0.4 for high-NO_x conditions
204 (Liu et al., 2018). Therefore, based on elemental ratios, the evolution in SOA composition measured in this study is
205 comparable to that in bulk average properties estimated by AMS. Furthermore, we use 2D-VBS framework developed
206 by Donahue et al. (2012) to investigate OA chemistry, and understand the evolution of cooking SOA through changes
207 in the volatility of SOA system. The vapor pressures of the identified compounds are calculated using group
208 contribution method (Pankow and Asher, 2008) where experimentally determined vapor pressures were unavailable,
209 and reported in Table S2. The observed compounds in SOA have a broad range of volatilities, since they were formed
210 from oxidation of a complex ensemble of VOC precursors. As shown in Fig. S6, there is minor decrease in overall
211 volatility of the mixture (change lies within one decade in C*) irrespective of the presence of peroxides, while $\overline{\text{O}:\text{C}}$
212 is increasing with oxidation. This increase in oxidation state is coincident with increasing fragmentation upon oxidation,
213 and, as a result, the overall change in the bulk volatility of canola oil SOA is relatively small.

214 As mentioned earlier in Sect. 2.2, there is a potential to misclassify ROOH as ROH using our current GC/MS method.
215 Here we further examine the chemical composition by assuming that each -O-[Si(CH₃)₃] group observed originates
216 from an -OOH group in the SOA, and to support this argument we show that derivatization of cumene hydroperoxide
217 (Sigma Aldrich Co.) is observed as TMS of hydroxy-cumene in our system as shown in Fig. S3. It should be noted
218 that replacing -OH with -OOH results in a higher estimate of O:C (and $\overline{\text{O}:\text{C}}$) but does not change H:C or carbon #.
219 Furthermore, since pseudo molecular ion fraction ($f_{M-15/73}$) for organic peroxides (needed for quantification) is
220 unknown, we assume that it is similar to those presented in Table S2. As shown in Fig. S7, if all observed -OH groups
221 are -OOH groups, the VK-slope is -0.15 which is similar to -0.19 calculated based on the no-peroxide assumption.
222 Similarly, Fig. S6 shows that this uncertainty in hydroxyl group identification has negligible effect on estimation of
223 vapor pressure or volatility in the 2D-VBS framework. Therefore, this potential misclassification of peroxide groups
224 may lead to an underestimation in O:C and $\overline{\text{O}:\text{C}}$, but is not expected to affect estimates of volatility and our general
225 conclusions about the importance of fragmentation reactions. In the future, analytical techniques such as extractive
226 electrospray ionization time-of-flight mass spectrometry (Lopez-Hilfiker et al., 2019) may be useful to better
227 understand the composition of peroxides from cooking SOA. While the misclassification of peroxides may have little
228 impact on the bulk properties such as average O:C ratios, there may be important implications on understanding the
229 reactivity of the SOA.

230

231 3.2 Evaporation rates of SOA

232 The volatility of the SOA is also probed by measuring the evaporation rates in a heated thermodenuder and compared
233 to the rates expected from the measured composition. In order to derive the evaporation rates from the measured
234 chemical composition of cooking SOA, we use the kinetic mass transfer model developed by Riipinen et al. (2010).
235 Among the inputs into the model, the mass accommodation coefficient is a critical but uncertain parameter that
236 accounts for the mass transfer limitations in the system.



237 Figure 5 shows both measured and modeled mass thermograms for canola oil
238 SOA, mass accommodation coefficient of 0.03 is needed to predict the experimentally determined mass thermograms.
239 An accommodation coefficient of <1 suggests that mass transfer limitations in the system likely occurring in the
240 condensed-phase. Formation of multifunctional organic compounds such as those observed in this study is likely
241 responsible for an increase in viscosity through increasing hydrogen bonding and other polar interactions (Rothfuss
242 and Petters, 2016). It should be noted that Takhar et al. (2019) reported similar magnitudes of mass accommodation
243 coefficients for heterogeneous oxidation of cooking oil particles. Due to similarity in the type of functional groups
244 present in both aging pathways, we believe the decrease in mass accommodation coefficients for both systems undergo
245 similar changes in phase and/or viscosity.

246 These measurements of evaporation rates are consistent with the volatilities expected from our measured composition
247 of SOA containing small oxygenated compounds. Although mass accommodation coefficients are highly uncertain,
248 the mass accommodation coefficients for other SOA systems have been measured to be even lower on the order of 10^{-4}
249 (Cappa and Wilson, 2011), which would require the volatilities to be even higher to explain the measured evaporation
250 rates. Therefore, the TD measurements support the conclusion that smaller oxygenated compounds are produced from
251 oxidation of cooking oil vapors, and that fragmentation reactions are dominant. Furthermore, these measurements
252 provide useful inputs into chemical transport models for predicting SOA formation and gas-particle partitioning. Our
253 previous work (Takhar et al., 2019) showed that even at $\alpha = 10^{-2}$, gas-particle partitioning timescales are short (within
254 hours) and the assumption of equilibrium partitioning still holds for regional scale SOA formation. Further work is
255 needed to directly measure the viscosity of cooking SOA, and corresponding mixing timescales to better constrain the
256 physicochemical properties of cooking SOA.

257

258 3.3 Contribution of aldehydes to observed oxidation products and total SOA

259 Since cooking oil vapors are comprised of a number of reactive aldehydes that can lead to SOA formation, we conduct
260 further experiments of SOA formation from these precursors and identify the relative contributions to observed
261 oxidation products and to total SOA. These results are applied to the heated cooking oil experiments to understand the
262 role of aldehydes in the overall production and evolution of cooking oil SOA.

263 3.3.1 Formation of particle-phase oxidation products

264 As described in the earlier sections, we are able to quantify the mass concentrations of different compound groups (6
265 different combinations of functional groups, from C2 to C9, summarized in Table S2) in the particle phase for all
266 experiments. We denote the observed mass concentrations of compound group i in SOA from canola oil
267 photooxidation as M_i^{oil} . The expected precursors to these oxidation products are likely aldehydes, since aldehydes are
268 emitted in significant amounts and are highly reactive. To examine this hypothesis, here we calculate the formation
269 of these observed compound groups from oxidation of aldehydes. For this calculation, heptanal, *trans*-2-heptenal,
270 *trans*-2-octenal, and *trans,trans*-2,4-heptadienal (Sigma Aldrich Co.) were considered because these aldehydes are the



271 dominant VOC precursors emitted from heated canola oil in our experiments as shown in Fig. S8. Unlike previous
272 work by Fullana et al. (2004b) and Klein et al. (2016a), gas-phase concentrations of decadienals were minimal in our
273 experiments. More volatile aldehydes, such as acrolein and methacrolein, were likely present but could not be captured
274 and analyzed by our techniques. The molar amount reacted for each aldehyde j in the canola oil oxidation experiments
275 is denoted as ΔVOC_j^{oil} , and was calculated based on the measured OH exposure.

276 In order to estimate the contribution from oxidation of an aldehyde j in the gas-phase mix to the formation of each
277 compound group i , we conducted a series of experiments in which a representative aldehyde was oxidized, and the
278 molar yields of the various compounds were measured:

$$279 \quad \gamma_{ij} = \frac{M_{ij}^{ind}/MW_i}{\Delta VOC_j^{ind}} \quad (3)$$

280 where γ_{ij} represents the molar yield of compound group i from precursor j , M_{ij}^{ind} denotes the mass concentration of
281 compound i observed in photooxidation experiments in which aldehyde j was the sole precursor, MW_i is the molecular
282 weight of compound i , and ΔVOC_j^{ind} is the amount of precursor j reacted in each experiment. γ_{ij} is then applied to the
283 heated cooking oil experiments to estimate the amount of oxidation products that would form from each precursor:

$$284 \quad M_i^{sum} = \sum_j \gamma_{ij} \Delta VOC_j^{oil} MW_i \quad (4)$$

285 A sample calculation for this analysis is presented in Sect. 3 of SI. The comparison between M_i^{sum} (contribution of
286 aldehyde oxidation to formation of compound i) and M_i^{oil} (observed concentrations of compound i) is shown in Fig.
287 6. Based on this methodology, oxidation of aldehydes accounts for $56 \mu\text{g m}^{-3}$ (M_i^{sum}) of the observed $75 \mu\text{g m}^{-3}$ (M_i^{oil})
288 (or 75%) particle-phase oxidation products measured at an OH exposure of 6.43×10^{10} molecules cm^{-3} s. The
289 contributions of alkanals (heptanal), alkenals (heptenal + octenal) and alkadienals (heptadienal) are 7%, ~31% and
290 37%, respectively.

291 While the amount of oxidation products expected from aldehydes is somewhat lower than that observed in canola oil
292 SOA, this difference may arise from differences in gas-particle partitioning between single aldehyde photooxidation
293 and canola oil photooxidation. As shown in Fig. S9, more oxygenated compounds (higher O:C and greater number of
294 functional groups) tend to be more abundant in the canola oil SOA than expected from aldehyde photooxidation,
295 suggesting that canola oil SOA is more favorable for oxygenated compounds to partition than SOA from individual
296 aldehydes. On the other hand, there is no clear trend in partitioning with respect to vapor pressures and carbon number.
297 It should be noted that uncertainties in the fitting procedure or estimation in the pseudo molecular ion (refer to Table
298 S2 and Fig. S5) can also result in uncertainties between -40% and +20%. Therefore, in summary, the quantified
299 oxidation products from canola oil SOA are generally consistent with those from aldehyde photooxidation, and the
300 relative amounts may be subject to further changes due to gas-particle partitioning.

301



302 3.3.2 Using the statistical oxidation model (SOM) framework

303 To further explore the evolution of canola oil SOA, we applied our results to the statistical oxidation model (SOM)
304 framework developed by Cappa and Wilson (Cappa et al., 2013; Cappa and Wilson, 2012). SOM describes the
305 oxidation chemistry of a VOC precursor through multi-generational space defined by the number of carbon and
306 oxygen atoms present in the precursor and its possible SOA product molecules. The SOM does not specifically track
307 the product composition in terms of functional groups, but provides adequate details to represent key atmospheric
308 processes such as gas-particle partitioning, fragmentation, functionalization, reactions with oxidants, condensed-phase
309 chemistry. The model has been applied to chamber experiments to derive parameterizations by fitting experimental
310 data to both SOA mass concentration and the bulk aerosol O/C ratio. Eluri et al. (2018) used the chamber derived
311 parameterizations to predict the properties of SOA generated from diesel exhaust in an oxidation flow tube reactor.

312 To the best of the authors' knowledge, there are no parameterizations for the oxidation of aldehydes. Therefore, in
313 this study we first derived the parameterizations for aldehyde oxidation, and then use these parameters to predict the
314 SOA mass concentrations. In order to obtain the parameters, we fit the measured SOA concentration from oxidation
315 of heptanal, *trans*-2-heptenal, *trans,trans*-2,4-heptadienal at different OH exposures to optimize the six tunable
316 parameters under low-NO_x conditions (shown in Fig. S10). Best fit SOM parameters indicate that photooxidation
317 leads to fragmentation per reaction with OH, as shown by a lower *mfrag* than compared to other systems e.g. alkanes
318 (≥ 2 for branched, cyclic or *n*-alkane under low-NO_x conditions (Eluri et al., 2018)). Since a lower value for *mfrag*
319 represents greater fragmentation (Cappa and Wilson, 2012), this again reflects the higher propensity for fragmentation
320 in this SOA system. The optimized parameters were then used to predict the SOA concentration for canola oil
321 photooxidation under different aging conditions.

322 Based on these established parameterizations for different aldehydes, model simulations were conducted for canola
323 oil having a mixture of aldehydes under different photochemical aging conditions. It should be noted that we used
324 parameterizations of heptanal for all alkanals, heptenal for all alkenals, and heptadienal for alkadienals. As shown in
325 Fig. 7, the model generally captures the amount of SOA formed to within 50%, but overpredicts SOA formation at
326 lower photochemical ages and underpredicts SOA concentrations at higher photochemical ages. In addition, SOM
327 also tracks atomic O/C ratio which were further compared with the measured O/C ratio. SOM predicts an O:C around
328 0.7, which lies within $\pm 20\%$ of the measured O:C likely suggesting that the changes in chemical composition of
329 cooking SOA is in good agreement with the model predictions.

330 One inconsistency between the model and measurements is the slope at which SOA is being formed. The experimental
331 data suggest a steeper trend of SOA formation while the model predicts a more gradual increase in SOA formation. A
332 potential explanation for this discrepancy is the contribution from other unmeasured VOCs. These VOCs are less
333 reactive than those considered in the model, such that they contribute to higher SOA at higher OH exposures.
334 Alternatively, these missing VOCs are more volatile such that more of their SOA is formed at later generations of
335 oxidation. For example, acrolein forms SOA with measurable yields (Chan et al., 2010) and is emitted at large amounts
336 from heated cooking oils (Klein et al., 2016a). Despite these limitations, these parameterizations generally capture the



337 amount of SOA formed and its degree of oxidation (O/C) on oxidation timescales relevant to urban areas (within 2
338 days) and are useful for representing cooking oil emissions in the chemical transport models. Overall, the amount of
339 SOA formed and the evolution upon oxidation can be well described by photooxidation of aldehydes.

340

341 **4 Conclusions and implications**

342 In this work, we characterized the detailed chemical composition of SOA generated from cooking oil vapors. We
343 showed that cooking SOA occurring as highly complex mixture can be deconvoluted using mass spectral
344 fragmentation pattern to extract useful information about the chemical identities of organic compounds, such as
345 functional groups and carbon number. Using this detailed chemical composition of cooking SOA, we showed that
346 fragmentation is an important pathway for oxidative processing of cooking emissions in the atmosphere even within
347 short timescales of oxidation. Furthermore, we showed that aldehydes can reasonably explain the formation of SOA
348 generated from cooking oil vapors and the oxidative evolution as described using a multi-generational oxidation
349 model. Our study, therefore, highlights the importance of molecular composition in constraining the chemical
350 properties of cooking SOA, as well as understanding the contribution of aldehydes in formation of SOA from cooking
351 emissions.

352 Consistent with other studies, our work has shown that aldehydes are an important class of VOC precursors emitted
353 from cooking emissions, and substantial efforts have been made to measure their emission factors depending on
354 different cooking settings (heating temperature, cooking style, food, ingredients) (Klein et al., 2016a, 2016b).
355 However, the contribution of aldehydes from cooking emissions is underrepresented in chemical transport models.
356 Recently, McDonald et al. (2018) showed that the ambient concentrations of OA were underpredicted when aldehydes
357 were not included in the box model calculations, suggesting that aldehydes, likely from food cooking, play an
358 important role in atmospheric oxidation chemistry. Furthermore, Klein et al. (2019) showed that heavy pollutants like
359 restaurants play a significant role in contributing to the ambient cooking organic aerosol concentrations. In this study,
360 we showed a large fraction of the SOA is derived from aldehyde precursors, with strong similarities in chemical
361 composition. Therefore, it is important to consider the contribution of aldehyde chemistry in atmospheric models
362 towards total OA budget. Furthermore, we demonstrated the importance of fragmentation reactions and their influence
363 on OA properties such as volatility and chemical composition. Future work should therefore focus on measuring not
364 only the SOA formation, but also the oxygenated VOCs formed due to fragmentation upon aging to provide insights
365 into aging of cooking emissions.

366 Gas-particle partitioning of SOA can be further affected by non-ideal mixing, as well as morphology of the particles
367 (Shiraiwa et al., 2013; Zuend and Seinfeld, 2012). Future work should investigate the effect of these parameters on
368 cooking SOA properties and formation potential. To account for thermodynamic mixing favourability of the particles,
369 Hansen solubility framework developed by Ye et al. (2016) can be implemented to provide insights into SOA mixing
370 and yield enhancement. As shown in Ye et al. (2018) primary meat-cooking emissions can enhance SOA yield from
371 α -pinene due to similarity in Hansen solubility parameters suggesting that primary meat cooking particles are miscible



372 with α -pinene SOA. It should be noted that present study did not investigate the effect of atmospherically relevant
373 seed particles as well as NO_x levels which are representative of typical urban environments. Since emissions upon
374 entering the atmosphere gets mixed with background air, other source emissions, and diluted upon mixing thereby
375 altering the gas-particle partitioning, and thus the total OA loading. Therefore, it is important to understand the changes
376 in partitioning and miscibility of cooking emissions as the composition continually evolves with atmospheric
377 processing. Additionally, as mentioned earlier cooking SOA undergoes large mass transfer limitations due to changes
378 in the phase state of the SOA particles, making it more so important to experimentally determine the corresponding
379 viscosity of cooking SOA. Therefore, future work should focus on measuring both the viscosity and miscibility of
380 SOA derived from cooking emissions.

381

382 *Data availability.* The data are available upon request to the corresponding author.

383

384 *Competing interests.* The authors declare that they have no conflict of interests.

385

386 *Acknowledgements.* The authors acknowledge Environment and Climate Change Canada (ECCC) for funding support
387 through the Government of Canada Grants and Contribution program. The authors would like to thank Shao-Meng Li
388 from ECCC for use of the thermodenuder, Chris Cappa from UC Davis for help with SOM simulations, Greg Evans,
389 Jeff Brook and Tengyu Liu from University of Toronto for helpful discussion.



390 References

- 391 Allan, J. D., Williams, P. I., Morgan, W. T., Martin, C. L., Flynn, M. J., Lee, J., Nemitz, E., Phillips, G. J.,
392 Gallagher, M. W. and Coe, H.: Contributions from transport, solid fuel burning and cooking to primary organic
393 aerosols in two UK cities, *Atmos. Chem. Phys.*, 10(2), 647–668, doi:10.5194/acp-10-647-2010, 2010.
- 394 Canagaratna, M. R., Jimenez, J. L., Kroll, J. H., Chen, Q., Kessler, S. H., Massoli, P., Hildebrandt Ruiz, L., Fortner,
395 E., Williams, L. R., Wilson, K. R., Surratt, J. D., Donahue, N. M., Jayne, J. T. and Worsnop, D. R.: Elemental ratio
396 measurements of organic compounds using aerosol mass spectrometry: Characterization, improved calibration, and
397 implications, *Atmos. Chem. Phys.*, 15(1), 253–272, doi:10.5194/acp-15-253-2015, 2015.
- 398 Cappa, C. D. and Wilson, K. R.: Evolution of organic aerosol mass spectra upon heating: Implications for OA phase
399 and partitioning behavior, *Atmos. Chem. Phys.*, 11(5), 1895–1911, doi:10.5194/acp-11-1895-2011, 2011.
- 400 Cappa, C. D. and Wilson, K. R.: Multi-generation gas-phase oxidation, equilibrium partitioning, and the formation
401 and evolution of secondary organic aerosol, *Atmos. Chem. Phys.*, 12(20), 9505–9528, doi:10.5194/acp-12-9505-
402 2012, 2012.
- 403 Cappa, C. D., Zhang, X., Loza, C. L., Craven, J. S., Yee, L. D. and Seinfeld, J. H.: Application of the Statistical
404 Oxidation Model (SOM) to Secondary Organic Aerosol formation from photooxidation of C12 alkanes, *Atmos.*
405 *Chem. Phys.*, 13(3), 1591–1606, doi:10.5194/acp-13-1591-2013, 2013.
- 406 Chan, A. W. H., Chan, M. N., Surratt, J. D., Chhabra, P. S., Loza, C. L., Crouse, J. D., Yee, L. D., Flagan, R. C.,
407 Wennberg, P. O. and Seinfeld, J. H.: Role of aldehyde chemistry and NO_x concentrations in secondary organic
408 aerosol formation, *Atmos. Chem. Phys.*, 10(15), 7169–7188, doi:10.5194/acp-10-7169-2010, 2010.
- 409 Choe, E. and Min, D. B.: Mechanisms and factors for edible oil oxidation, *Compr. Rev. Food Sci. Food Saf.*, 5(4),
410 169–186, doi:10.1111/j.1541-4337.2006.00009.x, 2006.
- 411 Choe, E. and Min, D. B.: Chemistry of deep-fat frying oils, *J. Food Sci.*, 72(5), doi:10.1111/j.1750-
412 3841.2007.00352.x, 2007.
- 413 Crippa, M., Decarlo, P. F., Slowik, J. G., Mohr, C., Heringa, M. F., Chirico, R., Poulain, L., Freutel, F., Sciare, J.,
414 Cozic, J., Di Marco, C. F., Elsasser, M., Nicolas, J. B., Marchand, N., Abidi, E., Wiedensohler, A., Drewnick, F.,
415 Schneider, J., Borrmann, S., Nemitz, E., Zimmermann, R., Jaffrezo, J.-L., Prevot, A. S. H. and Baltensperger, U.:
416 Wintertime aerosol chemical composition and source apportionment of the organic fraction in the metropolitan area
417 of Paris, *Atmos. Chem. Phys.*, 13(2), 961–981, doi:10.5194/acp-13-961-2013, 2013.
- 418 Dall’Osto, M., Paglione, M., Decesari, S., Facchini, M. C., O’Dowd, C., Plass-Duellmer, C. and Harrison, R. M.: On
419 the Origin of AMS “cooking Organic Aerosol” at a Rural Site, *Environ. Sci. Technol.*, 49(24), 13964–13972,
420 doi:10.1021/acs.est.5b02922, 2015.
- 421 Donahue, N. M., Robinson, A. L., Stanier, C. O. and Pandis, S. N.: Coupled partitioning, dilution, and chemical
422 aging of semivolatile organics, *Environ. Sci. Technol.*, 40(8), 2635–2643, doi:10.1021/es052297c, 2006.
- 423 Donahue, N. M., Kroll, J. H., Pandis, S. N. and Robinson, A. L.: A two-dimensional volatility basis set-Part 2:
424 Diagnostics of organic-aerosol evolution, *Atmos. Chem. Phys.*, 12(2), 615–634, doi:10.5194/acp-12-615-2012,
425 2012.
- 426 Eluri, S., Cappa, C. D., Friedman, B., Farmer, D. K. and Jathar, S. H.: Modeling the formation and composition of
427 secondary organic aerosol from diesel exhaust using parameterized and semi-explicit chemistry and thermodynamic
428 models, *Atmos. Chem. Phys.*, 18(19), 13813–13838, doi:10.5194/acp-18-13813-2018, 2018.
- 429 Florou, K., Papanastasiou, D. K., Pikridas, M., Kaltsonoudis, C., Louvaris, E., Gkatzelis, G. I., Patoulias, D.,
430 Mihalopoulos, N. and Pandis, S. N.: The contribution of wood burning and other pollution sources to wintertime
431 organic aerosol levels in two Greek cities, *Atmos. Chem. Phys.*, 17(4), 3145–3163, doi:10.5194/acp-17-3145-2017,
432 2017.



- 433 Fullana, A., Carbonell-Barrachina, A. A. and Sidhu, S.: Comparison of volatile aldehydes present in the cooking
434 fumes of extra virgin olive, olive, and canola oils, *J. Agric. Food Chem.*, 52(16), 5207–5214, doi:10.1021/jf035241f,
435 2004a.
- 436 Fullana, A., Carbonell-Barrachina, A. A. and Sidhu, S.: Volatile aldehyde emissions from heated cooking oils, *J.*
437 *Sci. Food Agric.*, 84(15), 2015–2021, doi:10.1002/jsfa.1904, 2004b.
- 438 Gardner, H. W.: Oxygen radical chemistry of polyunsaturated fatty acids, *Free Radic. Biol. Med.*, 7(1), 65–86,
439 doi:10.1016/0891-5849(89)90102-0, 1989.
- 440 Hallquist, M., Wenger, J. C., Baltensperger, U., Rudich, Y., Simpson, D., Claeys, M., Dommen, J., Donahue, N. M.,
441 George, C., Goldstein, A. H., Hamilton, J. F., Herrmann, H., Hoffmann, T., Iinuma, Y., Jang, M., Jenkin, M. E.,
442 Jimenez, J. L., Kiendler-Scharr, J., Maenhaut, W., McFiggans, G., Mentel, T. F., Monod, A., Prevot, A. S. H.,
443 Seinfeld, J. H., Surratt, J. D., Szmigielski, R. and Wildt, J.: The formation, properties and impact of secondary
444 organic aerosol: current and emerging issues, *Atmos. Chem. Phys.*, 9(14), 5155–5236, doi:10.5194/acp-9-5155-
445 2009, 2009.
- 446 Hayes, P. L., Ortega, A. M., Cubison, M. J., Froyd, K. D., Zhao, Y., Cliff, S. S., Hu, W. W., Toohey, D. W., Flynn,
447 J. H., Lefer, B. L., Grossberg, N., Alvarez, S., Rappenglück, B., Taylor, J. W., Allan, J. D., Holloway, J. S., Gilman,
448 J. B., Kuster, W. C., De Gouw, J. A., Massoli, P., Zhang, X., Liu, J., Weber, R. J., Corrigan, A. L., Russell, L. M.,
449 Isaacman, G., Worton, D. R., Kreisberg, N. M., Goldstein, A. H., Thalman, R., Waxman, E. M., Volkamer, R., Lin,
450 Y. H., Surratt, J. D., Kleindienst, T. E., Offenberg, J. H., Dusanter, S., Griffith, S., Stevens, P. S., Brioude, J.,
451 Angevine, W. M. and Jimenez, J. L.: Organic aerosol composition and sources in Pasadena, California, during the
452 2010 CalNex campaign, *J. Geophys. Res. Atmos.*, 118(16), 9233–9257, doi:10.1002/jgrd.50530, 2013.
- 453 Heald, C. L., Kroll, J. H., Jimenez, J. L., Docherty, K. S., Decarlo, P. F., Aiken, A. C., Chen, Q., Martin, S. T.,
454 Farmer, D. K. and Artaxo, P.: A simplified description of the evolution of organic aerosol composition in the
455 atmosphere, *Geophys. Res. Lett.*, 37(8), doi:10.1029/2010GL042737, 2010.
- 456 Huang, X., He, L., Hu, M., Canagaratna, M. R., Sun, Y., Zhang, Q., Zhu, T., Xue, L., Zeng, L. W., Liu, X. G.,
457 Zhang, Y. H., Jayne, J. T., Ng, N. L. and Worsnop, D. R.: and Physics Highly time-resolved chemical
458 characterization of atmospheric submicron particles during 2008 Beijing Olympic Games using an Aerodyne High-
459 Resolution Aerosol Mass Spectrometer, *Atmos. Chem. Phys.*, 10(18), 8933–8945, doi:10.5194/acp-10-8933-2010,
460 2010.
- 461 Isaacman-VanWertz, G., Lu, X., Weiner, E., Smiley, E. B. and Widdowson, M. A.: Characterization of hydrocarbon
462 groups in complex mixtures using gas chromatography with unit-mass resolution electron ionization mass
463 spectrometry, *Anal. Chem.*, 92(18), 12481–12488, doi:10.1021/acs.analchem.0c02308, 2020.
- 464 Jaoui, M., Kleindienst, T. E., Lewandowski, M. and Edney, E. O.: Identification and quantification of aerosol polar
465 oxygenated compounds bearing carboxylic or hydroxyl groups. 1. Method development, *Anal. Chem.*, 76(16),
466 4765–4778, doi:10.1021/ac049919h, 2004.
- 467 Jaoui, M., Kleindienst, T. E., Lewandowski, M., Offenberg, J. H. and Edney, E. O.: Identification and quantification
468 of aerosol polar oxygenated compounds bearing carboxylic or hydroxyl groups. 2. Organic tracer compounds from
469 monoterpenes, *Environ. Sci. Technol.*, 39(15), 5661–5673, doi:10.1021/es048111b, 2005.
- 470 Kaltsonoudis, C., Kostenidou, E., Louvaris, E., Psychoudaki, M., Tsiligiannis, E., Florou, K., Liangou, A. and
471 Pandis, S. N.: Characterization of fresh and aged organic aerosol emissions from meat charbroiling, *Atmos. Chem.*
472 *Phys.*, 17(11), 7143–7155, doi:10.5194/acp-17-7143-2017, 2017a.
- 473 Kaltsonoudis, C., Kostenidou, E., Louvaris, E., Psychoudaki, M., Tsiligiannis, E., Florou, K., Liangou, A. and
474 Pandis, S. N.: Characterization of fresh and aged organic aerosol emissions from meat charbroiling, *Atmos. Chem.*
475 *Phys.*, 17(11), 7143–7155, doi:10.5194/acp-17-7143-2017, 2017b.
- 476 Katragadda, H. R., Fullana, A., Sidhu, S. and Carbonell-Barrachina, A. A.: Emissions of volatile aldehydes from
477 heated cooking oils, *Food Chem.*, 120(1), 59–65, doi:10.1016/j.foodchem.2009.09.070, 2010.



- 478 Klein, F., Platt, S. M., Farren, N. J., Detournay, A., Bruns, E. A., Bozzetti, C., Daellenbach, K. R., Kilic, D., Kumar,
479 N. K., Pieber, S. M., Slowik, J. G., Temime-roussel, B., Marchand, N., Hamilton, J. F., Baltensperger, U., Prévôt, A.
480 S. H. and El Haddad, I.: Characterization of Gas-Phase Organics Using Proton Transfer Reaction Time-of-Flight
481 Mass Spectrometry: Cooking Emissions, *Environ. Sci. Technol.*, 50(3), 1243–1250, doi:10.1021/acs.est.5b04618,
482 2016a.
- 483 Klein, F., Farren, N. J., Bozzetti, C., Daellenbach, K. R., Kilic, D., Kumar, N. K., Pieber, S. M., Slowik, J. G.,
484 Tuthill, R. N., Hamilton, J. F., Baltensperger, U., Prévôt, A. S. H. and El Haddad, I.: Indoor terpene emissions from
485 cooking with herbs and pepper and their secondary organic aerosol production potential, *Sci. Rep.*, 6, 1–7,
486 doi:10.1038/srep36623, 2016b.
- 487 Klein, F., Baltensperger, U., Prévôt, A. S. H. and El Haddad, I.: Quantification of the impact of cooking processes
488 on indoor concentrations of volatile organic species and primary and secondary organic aerosols, *Indoor Air*, 29(6),
489 926–942, doi:10.1111/ina.12597, 2019.
- 490 Kostenidou, E., Florou, K., Kaltsonoudis, C., Tsiflikiotou, M., Vratolis, S., Eleftheriadis, K. and Pandis, S. N.:
491 Sources and chemical characterization of organic aerosol during the summer in the eastern Mediterranean, *Atmos.*
492 *Chem. Phys.*, 15(19), 11355–11371, doi:10.5194/acp-15-11355-2015, 2015.
- 493 Kroll, J. H., Donahue, N. M., Jimenez, J. L., Kessler, S. H., Canagaratna, M. R., Wilson, K. R., Altieri, K. E.,
494 Mazzoleni, L. R., Wozniak, A. S., Bluhm, H., Mysak, E. R., Smith, J. D., Kolb, C. E. and Worsnop, D. R.: Carbon
495 oxidation state as a metric for describing the chemistry of atmospheric organic aerosol, *Nat. Chem.*, 3(2), 133–139,
496 doi:10.1038/nchem.948, 2011.
- 497 Lambe, A. T., Onasch, T. B., Croasdale, D. R., Wright, J. P., Martin, A. T., Franklin, J. P., Massoli, P., Kroll, J. H.,
498 Canagaratna, M. R., Brune, W. H., Worsnop, D. R. and Davidovits, P.: Transitions from functionalization to
499 fragmentation reactions of laboratory Secondary Organic Aerosol (SOA) generated from the OH oxidation of alkane
500 precursors, *Environ. Sci. Technol.*, 46(10), 5430–5437, doi:10.1021/es300274t, 2012.
- 501 Lambe, A. T., Chhabra, P. S., Onasch, T. B., Brune, W. H., Hunter, J. F., Kroll, J. H., Cummings, M. J., Brogan, J.
502 F., Parmar, Y., Worsnop, D. R., Kolb, C. E. and Davidovits, P.: Effect of oxidant concentration, exposure time, and
503 seed particles on secondary organic aerosol chemical composition and yield, *Atmos. Chem. Phys.*, 15(6), 3063–
504 3075, doi:10.5194/acp-15-3063-2015, 2015.
- 505 Lee, B. P., Li, Y. J., Yu, J. Z., Louie, P. K. K. and Chan, C. K.: Characteristics of submicron particulate matter at the
506 urban roadside in downtown Hong Kong—overview of 4 months of continuous high-resolution aerosol mass
507 spectrometer measurements, *J. Geophys. Res.*, 120(14), 7040–7058, doi:10.1002/2015JD023311. Received, 2015.
- 508 Liu, T., Liu, Q., Li, Z., Huo, L., Chan, M. N., Li, X., Zhou, Z. and Chan, C. K.: Emission of volatile organic
509 compounds and production of secondary organic aerosol from stir-frying spices, *Sci. Total Environ.*, 599–600,
510 1614–1621, doi:10.1016/j.scitotenv.2017.05.147, 2017a.
- 511 Liu, T., Li, Z., Chan, M. and Chan, C. K.: Formation of secondary organic aerosols from gas-phase emissions of
512 heated cooking oils, *Atmos. Chem. Phys.*, 17(12), 7333–7344, doi:10.5194/acp-17-7333-2017, 2017b.
- 513 Liu, T., Wang, Z., Huang, D. D., Wang, X. and Chan, C. K.: Significant Production of Secondary Organic Aerosol
514 from Emissions of Heated Cooking Oils, *Environ. Sci. Technol. Lett.*, 5(1), 32–37, doi:10.1021/acs.estlett.7b00530,
515 2017c.
- 516 Liu, T., Wang, Z., Wang, X. and Chan, C. K.: Primary and secondary organic aerosol from heated cooking oil
517 emissions, *Atmos. Chem. Phys.*, 18(15), 11363–11374, doi:10.5194/acp-18-11363-2018, 2018.
- 518 Lopez-Hilfiker, F. D., Pospisilova, V., Huang, W., Kalberer, M., Mohr, C., Stefenelli, G., Thornton, J. A.,
519 Baltensperger, U., Prevot, A. S. H. and Slowik, J. G.: An Extractive Electrospray Ionization Time-of-Flight Mass
520 Spectrometer (EESI-TOF) for online measurement of atmospheric aerosol particles, *Atmos. Meas. Tech.*, 12(9), 1–
521 40, doi:10.5194/amt-2019-45, 2019.
- 522 Mao, J., Ren, X., Brune, W. H., Olson, J. R., Crawford, J. H., Fried, A., Huey, L. G., Cohen, R. C., Heikes, B.,



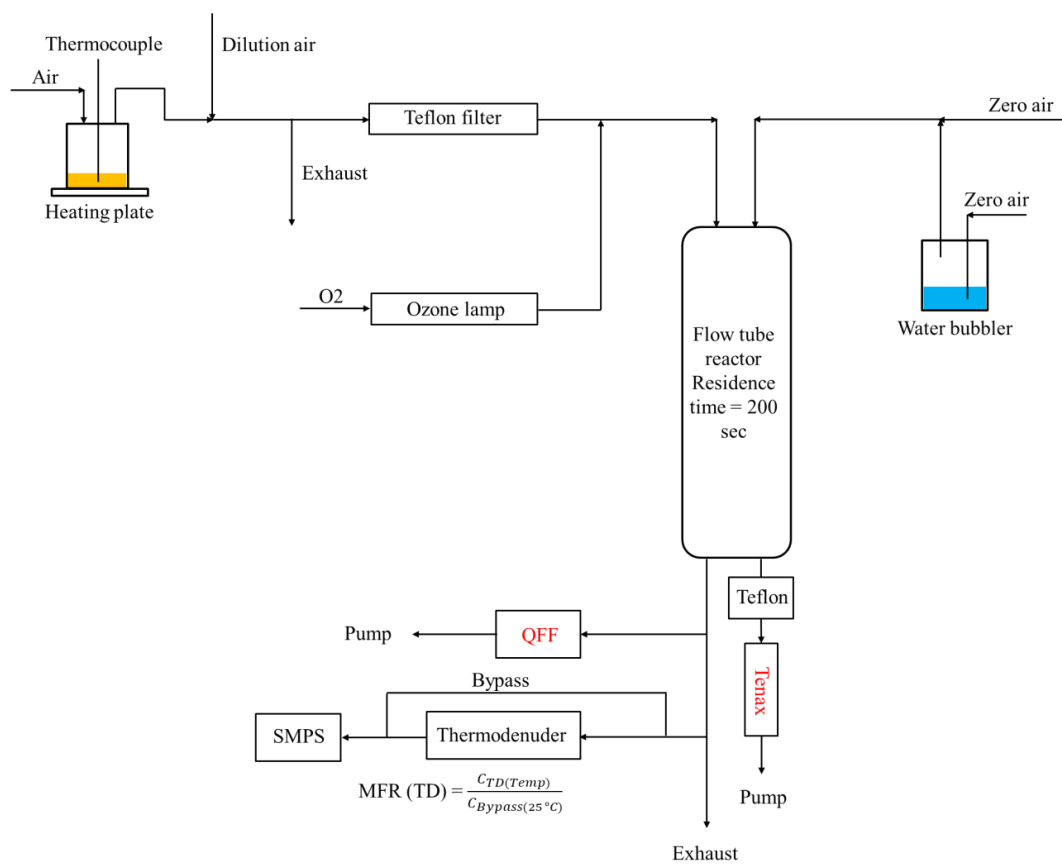
- 523 Singh, H. B., Blake, D. R., Sachse, G. W., Diskin, G. S., Hall, S. R. and Shetter, R. E.: Airborne measurement of
524 OH reactivity during INTEX-B, *Atmos. Chem. Phys.*, 9(1), 163–173, doi:10.5194/acp-9-163-2009, 2009.
- 525 McDonald, B. C., De Gouw, J. A., Gilman, J. B., Jathar, S. H., Akherati, A., Cappa, C. D., Jimenez, J. L., Lee-
526 Taylor, J., Hayes, P. L., McKeen, S. A., Cui, Y. Y., Kim, S. W., Gentner, D. R., Isaacman-VanWertz, G., Goldstein,
527 A. H., Harley, R. A. and Frost, M.: Volatile chemical products emerging as largest petrochemical source of urban
528 organic emissions, *Science* (80-.), 359(6377), 760–764, doi:10.1126/science.aaq0524, 2018.
- 529 Mohr, C., Huffman, J. A., Cubison, M. J., Aiken, A. C., Docherty, K. S., Kimmel, J. R., Ulbrich, I. M., Hannigan,
530 M. and Jimenez, J. L.: Characterization of primary organic aerosol emissions from meat cooking, trash burning, and
531 motor vehicles with high-resolution aerosol mass spectrometry and comparison with ambient and chamber
532 observations, *Environ. Sci. Technol.*, 43(7), 2443–2449, doi:10.1021/es8011518, 2009.
- 533 Mohr, C., Decarlo, P. F., Heringa, M. F., Chirico, R., Slowik, J. G., Richter, R., Reche, C., Alastuey, A., Querol, X.,
534 Seco, R., Penuelas, J., Jimenez, J. L., Crippa, M. , Zimmermann, R., Baltensperger, U. and Prévôt, A. S. H.:
535 Identification and quantification of organic aerosol from cooking and other sources in Barcelona using aerosol mass
536 spectrometer data, *Atmos. Chem. Phys.*, 12(4), 1649–1665, doi:10.5194/acp-12-1649-2012, 2012.
- 537 Pankow, J. F. and Asher, W. E.: SIMPOL.1: A simple group contribution method for predicting vapor pressures and
538 enthalpies of vaporization of multifunctional organic compounds, *Atmos. Chem. Phys.*, 8(10), 2773–2796,
539 doi:10.5194/acp-8-2773-2008, 2008.
- 540 Riipinen, I., Pierce, J. R., Donahue, N. M. and Pandis, S. N.: Equilibration time scales of organic aerosol inside
541 thermodenuders: Evaporation kinetics versus thermodynamics, *Atmos. Environ.*, 44(5), 597–607,
542 doi:10.1016/j.atmosenv.2009.11.022, 2010.
- 543 Rothfuss, N. E. and Petters, M. D.: Influence of functional groups on the viscosity of organic aerosol, *Environ. Sci.*
544 *Technol.*, 51(1), 271–279, doi:10.1021/acs.est.6b04478, 2016.
- 545 Schauer, J. J., Kleeman, M. J., Cass, G. R. and Simoneit, B. R. T.: Measurement of emissions from air pollution
546 sources. 1. C1 through C29 organic compounds from meat charbroiling, *Environ. Sci. Technol.*, 33(10), 1566–1577,
547 doi:10.1021/es980076j, 1999.
- 548 Schauer, J. J., Kleeman, M. J., Cass, G. R. and Simoneit, B. R. T.: Measurement of emissions from air pollution
549 sources. 4. C1-C27 organic compounds from cooking with seed oils, *Environ. Sci. Technol.*, 36(4), 567–575,
550 doi:10.1021/es002053m, 2002.
- 551 Shiraiwa, M., Zuend, A., Bertram, A. K. and Seinfeld, J. H.: Gas-particle partitioning of atmospheric aerosols:
552 Interplay of physical state, non-ideal mixing and morphology, *Phys. Chem. Chem. Phys.*, 15(27), 11441–11453,
553 doi:10.1039/c3cp51595h, 2013.
- 554 Sun, Y.-L., Zhang, Q., Schwab, J. J., Demerjian, K. L., Chen, W.-N., Bae, M.-S., Hung, H.-M., Hogrefe, O., Frank,
555 B., Rattigan, O. V. and Lin, Y.-C.: Characterization of the sources and processes of organic and inorganic aerosols
556 in New York city with a high-resolution time-of-flight aerosol mass spectrometer, *Atmos. Chem. Phys.*, 11(4),
557 1581–1602, doi:10.5194/acp-11-1581-2011, 2011.
- 558 Takhar, M., Stroud, C. A. and Chan, A. W. H.: Volatility Distribution and Evaporation Rates of Organic Aerosol
559 from Cooking Oils and their Evolution upon Heterogeneous Oxidation, *ACS Earth Sp. Chem.*, 3(9), 1717–1728,
560 doi:10.1021/acsearthspacechem.9b00110, 2019.
- 561 Ye, J., Gordon, C. A. and Chan, A. W. H.: Enhancement in Secondary Organic Aerosol Formation in the Presence
562 of Preexisting Organic Particle, *Environ. Sci. Technol.*, 50(7), 3572–3579, doi:10.1021/acs.est.5b05512, 2016.
- 563 Ye, J., Van Rooy, P., Adam, C. H., Jeong, C. H., Urch, B., Cocker, D. R., Evans, G. J. and Chan, A. W. H.:
564 Predicting Secondary Organic Aerosol Enhancement in the Presence of Atmospherically Relevant Organic Particles,
565 *ACS Earth Sp. Chem.*, 2(10), 1035–1046, doi:10.1021/acsearthspacechem.8b00093, 2018.
- 566 Yu, J., Flagan, R. C. and Seinfeld, J. H.: Identification of products containing -COOH, -OH, and -C=O in



- 567 atmospheric oxidation of hydrocarbons, *Environ. Sci. Technol.*, 32(16), 2357–2370, doi:10.1021/es980129x, 1998.
- 568 Zhao, Y., Hennigan, C. J., May, A. A., Tkacik, D. S., De Gouw, J. A., Gilman, J. B., Kuster, W. C., Borbon, A. and
569 Robinson, A. L.: Intermediate-volatility organic compounds: A large source of secondary organic aerosol, *Environ.*
570 *Sci. Technol.*, 48(23), 13743–13750, doi:10.1021/es5035188, 2014.
- 571 Zhao, Y., Nguyen, N. T., Presto, A. A., Hennigan, C. J., May, A. A. and Robinson, A. L.: Intermediate Volatility
572 Organic Compound Emissions from On-Road Diesel Vehicles: Chemical Composition, Emission Factors, and
573 Estimated Secondary Organic Aerosol Production, *Environ. Sci. Technol.*, 49(19), 11516–11526,
574 doi:10.1021/acs.est.5b02841, 2015.
- 575 Zuend, A. and Seinfeld, J. H.: Modeling the gas-particle partitioning of secondary organic aerosol: The importance
576 of liquid-liquid phase separation, *Atmos. Chem. Phys.*, 12(9), 3857–3882, doi:10.5194/acp-12-3857-2012, 2012.
- 577

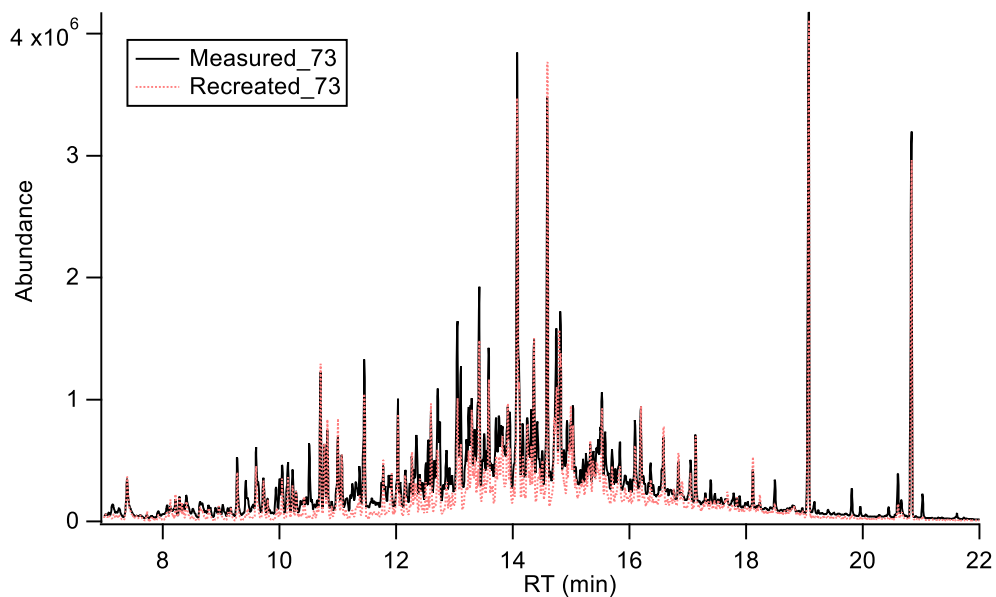


578



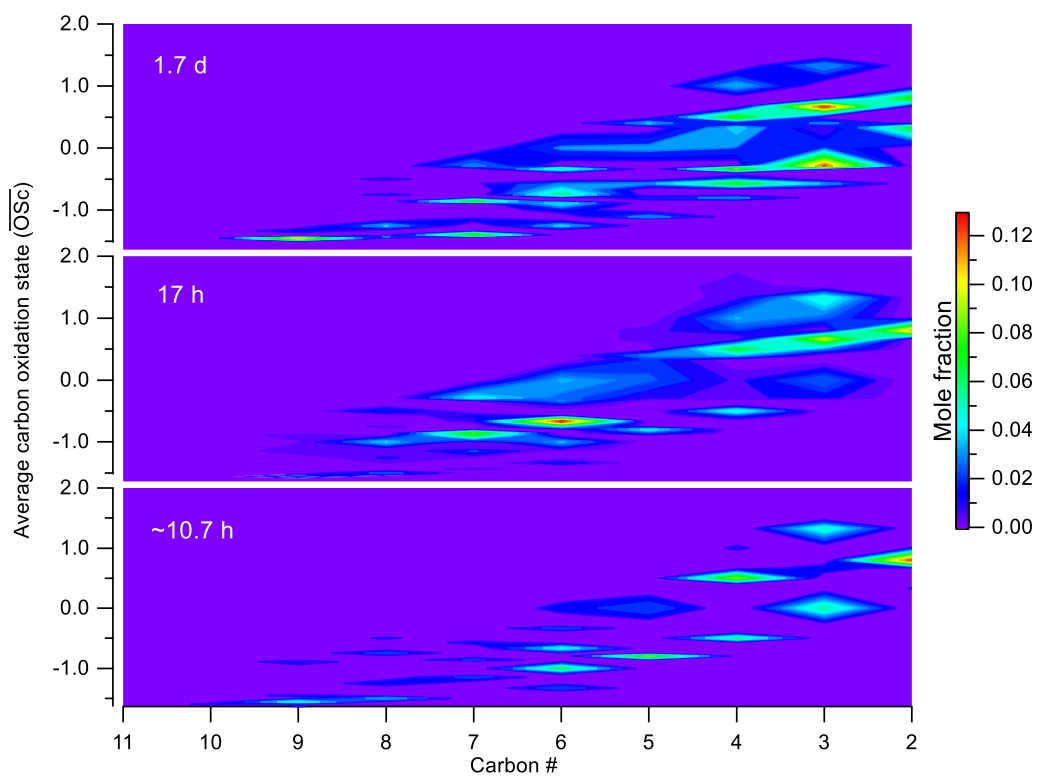
579

580 **Figure 1.** Experimental setup for oxidation of heated cooking oil emissions.



581

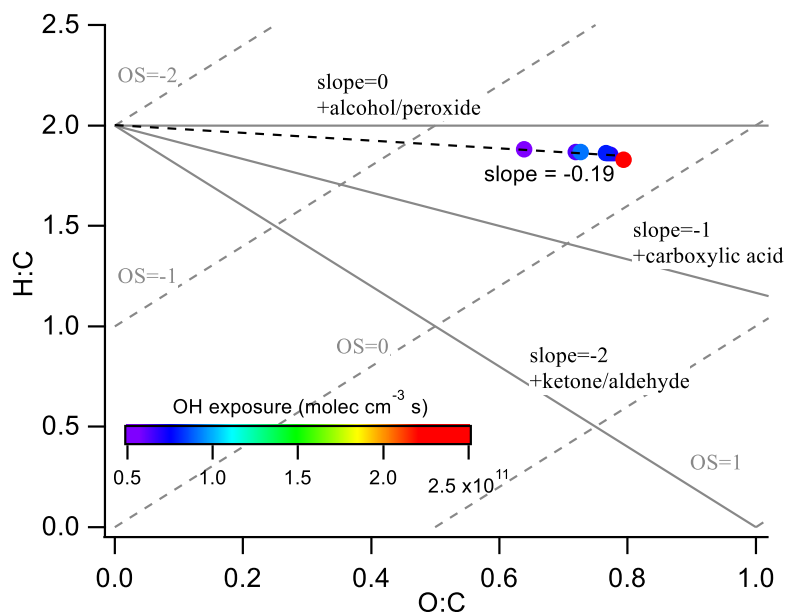
582 **Figure 2.** Highly complex mixture of canola oil SOA generated upon photooxidation. With known signal and mass fragmentation,
583 signal of m/z 73 can be recreated based on pseudo parent ions (e.g. M-15 used in this study).



584

585 **Figure 3.** Evolution in \overline{OSc} -nc space for canola oil SOA under different conditions of photochemical aging. As the oxidation
586 progresses in the atmosphere, more compounds are formed with smaller nc and higher \overline{OSc} suggesting fragmentation to be a
587 dominant pathway of oxidation for cooking emissions in the atmosphere.

588

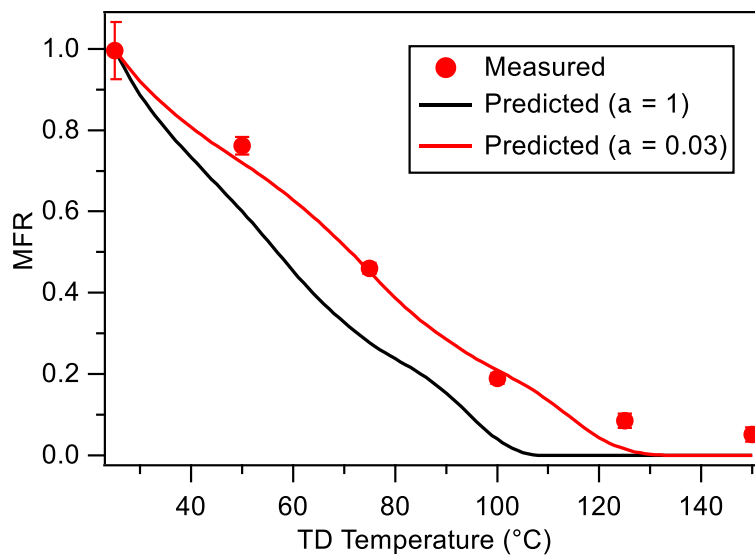


589

590 **Figure 4.** Van Krevelen diagram of canola oil SOA coloured by different OH exposure. In the background, average carbon
591 oxidation state (\overline{OS}_C) and functionalization slopes are shown for reference. The slope of -0.19 for canola oil SOA corresponds to
592 formation of both alcohol and carboxylic acid consistent with the chemical composition obtained from TD-GC/MS.



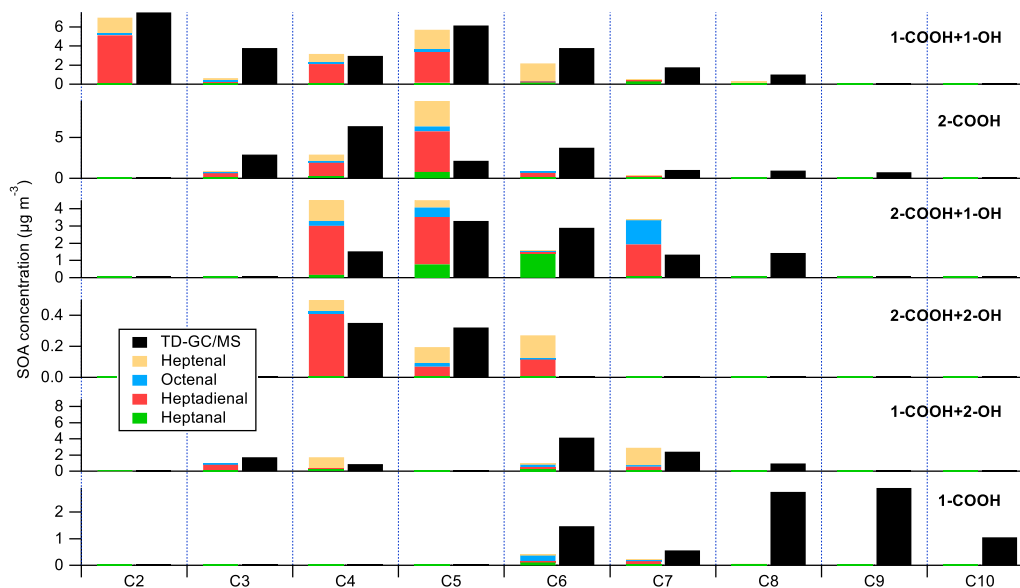
593



594

595 **Figure 5.** Mass thermogram of canola oil SOA at an OH exposure of 9.23×10^{10} molecules cm^{-3} s. The black line represents model
596 simulations using $\alpha = 1$ underpredicting the measured MFR. The red line corresponds to model simulations using $\alpha = 0.03$ predicting
597 the measurements reasonably well, therefore implying kinetic limitations in the system. The error bars represent $\pm 1\sigma$.

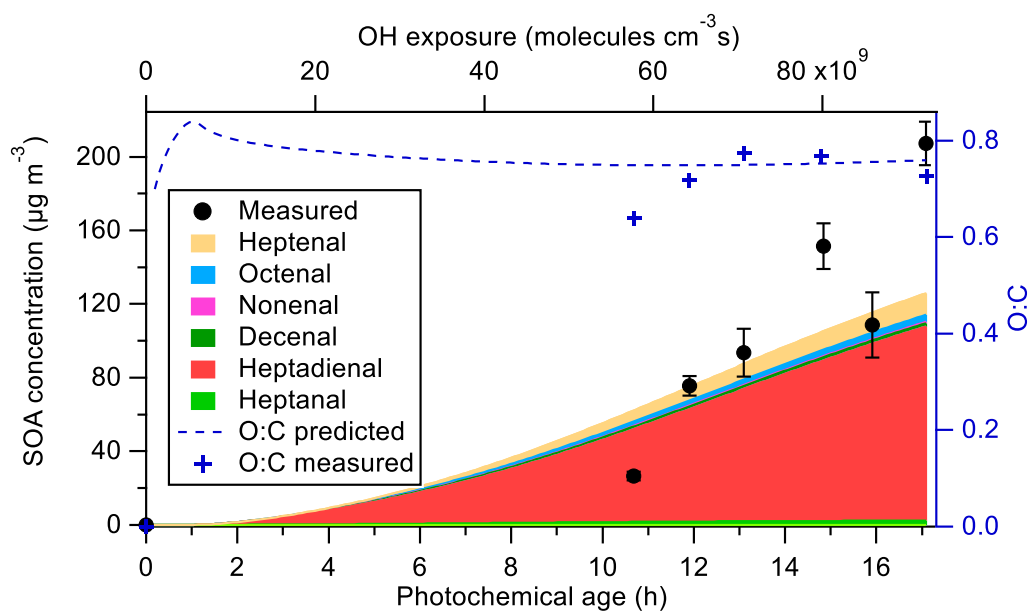
598



599

600 **Figure 6.** Prediction of different compounds formed at an OH exposure of 6.43×10^{10} molecules cm^{-3} s using product molar yields
601 of heptanal, heptenal, octenal, and heptadienal. The total aldehydes products can explain the observed oil SOA products within a
602 factor of half, while the inconsistency in prediction of some SOA products is likely caused by differences in gas-particle partitioning
603 in both photooxidation systems.

604



605

606 **Figure 7.** SOM prediction of SOA produced from different aldehydes with increasing photochemical age. The model overpredicts
607 SOA formation at lower photochemical age, while underpredicts SOA formation by ~40% at higher photochemical age, suggesting
608 that traditional VOC precursors cannot fully explain the SOA formation, and other gas-phase precursors maybe needed to better
609 constrain the formation of SOA at higher aging conditions. In addition, the SOM predicted O:C is within $\pm 20\%$ of the measured
610 O:C suggesting that the overall change in chemical composition of cooking SOA is predicted reasonably well.